Hindawi
Adsorption Science & Technology
Volume 2023, Article ID 9796065, 1 page
https://doi.org/10.1155/2023/9796065

Retraction

Retracted: Methylene Blue Dye Photodegradation during Synthesis and Characterization of WO_3 Nanoparticles

Adsorption Science and Technology

Received 19 December 2023; Accepted 19 December 2023; Published 20 December 2023

This article has been retracted by Hindawi following an investigation undertaken by the publisher [1]. This investigation has uncovered evidence of one or more of the following indicators of systematic manipulation of the publication process:

(1) Discrepancies in scope

(2) Discrepancies in the description of the research reported

(3) Discrepancies between the availability of data and the research described

(4) Inappropriate citations

(5) Incoherent, meaningless and/or irrelevant content included in the article

(6) Manipulated or compromised peer review

The presence of these indicators undermines our confidence in the integrity of the article's content and we cannot, therefore, vouch for its reliability. Please note that this notice is intended solely to alert readers that the content of this article is unreliable. We have not investigated whether authors were aware of or involved in the systematic manipulation of the publication process.

Wiley and Hindawi regrets that the usual quality checks did not identify these issues before publication and have since put additional measures in place to safeguard research integrity.

We wish to credit our own Research Integrity and Research Publishing teams and anonymous and named external researchers and research integrity experts for contributing to this investigation.

The corresponding author, as the representative of all authors, has been given the opportunity to register their agreement or disagreement to this retraction. We have kept a record of any response received.

References

[1] R. Surakasi, Alimuddin, Y. S. Rao et al., "Methylene Blue Dye Photodegradation during Synthesis and Characterization of WO_3 Nanoparticles," *Adsorption Science & Technology*, vol. 2022, Article ID 2882048, 10 pages, 2022.

Hindawi
Adsorption Science & Technology
Volume 2022, Article ID 2882048, 10 pages
https://doi.org/10.1155/2022/2882048

Research Article

Methylene Blue Dye Photodegradation during Synthesis and Characterization of WO_3 Nanoparticles

Raviteja Surakasi,[1] **Alimuddin**,[2] **Yenda Srinivasa Rao**,[3] **Ashitha K. Sanuj**,[4] **Pravin P. Patil**,[5] **A. Jayaganthan**,[6] **and Ramana Hechhu**[7]

[1]*Department of Mechanical Engineering, Lendi Institute of Engineering and Technology, Jonnada, Vizianagarm 535005, India*
[2]*Physical Sciences Section, School of Sciences, Maulana Azad National Urdu University, Hyderabad, 500032 Telangana, India*
[3]*Department of Mechanical Engineering, Swamy Vivekananda Engineering College, Bobbili, Andhra Pradesh, India*
[4]*Department of Microbiology, EMEA College, Malappuram, Kerala, India*
[5]*Mechanical Engineering Department, Graphic Era Deemed to be University, Dehradun, Uttarakhand, India*
[6]*Department of Automobile Engineering, Sathyabama Institute of Science and Technology, Chennai, Tamil Nadu, India*
[7]*Department of Pharmaceutical Chemistry, School of Pharmacy, Wolaita Sodo University, Ethiopia*

Correspondence should be addressed to Ramana Hechhu; ramana@wsu.edu.et

Received 18 May 2022; Revised 22 June 2022; Accepted 5 July 2022; Published 22 July 2022

Academic Editor: Jeevan Kumar Reddy Modigunta

Semiconductor-based photocatalytic systems have found widespread use in environmental pollution cleanup and renewable energy production. In this study, we synthesized WO_3 as a catalyst for the degradation of methylene blue, a thiazine dye, which was used in the previous work. The hydrothermal process is used to create WO_3 nanoparticles, which are made from sodium tungstate. When it comes to confirming the nanoparticles, many characterization techniques are employed, including X-ray diffraction (XRD), Fourier transform infrared (FTIR), UV-Vis diffuse reflectance spectrometer (DRS), X-ray photoelectron spectroscopy (XPS), and field emission–scanning electron microscope (FE-SEM). The existence of monoclinic crystalline structure is shown by XRD, with the average crystalline size being around 34 nm. FTIR confirms the presence of metal oxides. The pellucid absorption extremity in the UV-Vis region corresponds to the rudimentary absorption of the WO_3 semiconductor. FE-SEM confirms square-shaped nanoplates with EDX address the occurrence of elemental tungsten. The photocatalytic activity of WO_3 nanoparticles against methylene blue is taken for at different intervals of time that confirms MB's degradation. Our present work suggests that prepared nanoparticles should be potential for photocatalysts using various industrial dyes.

1. Introduction

Scientists use nanomaterials, which are little scientific particles. Even at the nanoscale, they retain their important qualities. The size and properties of nanoparticles make them ideal for a wide range of scientific applications [1]. In the near future, it will transform electronics, catalysis, sensor technology, adsorbents, and energy storage. When it comes to its many capabilities, the nanoparticle is described as a small portion of 1 to 100 nanometers in diameter that can function as a complete component [2]. Many different kinds of applications rely on their supercilious surface activity. They are vital to the development of world-class technology in the future [3]. Due to the growth and expansion of companies, populations, and dangerous goods, several environmental disasters are rising nowadays. These organic effluents, which are difficult to debase naturally, have a negative impact on marine ecosystems and human health [4]. Some processes such as chemical coagulation, flocculation, exchange, membrane filtration, and adsorption ion are used to rectify these contaminations; however, these processes transform them into new phases that have not yet been demolished [5]. As an alternative to all of the foregoing procedures, photocatalytic processes are widely acknowledged

as being a viable option for controlling these issues by altering their concentration. A photocatalyst must have an adequate bandgap, morphology, a large surface area, a high degree of strength, and the ability to be recycled [6]. Semiconductor-based photocatalytic devices are cost-effective and environmentally friendly, with broad absorption spectra that allow for a wide range of electron transmission processes, and without losing photocatalytic activity [7].

Applied photocatalysis relies heavily on the utilisation of metal oxides, which have a promising electrical structure and light absorption properties. As compared to ZnO, SnO2, TiO2, and CdO, tungsten trioxide WO_3 is an n-type semiconductor promising material for photocatalytic activity that meets all of the properties described above. Among its many potential uses are field electron emission devices, gas detectors, biosensors, chromophores, and windows with photocatalytic activity [8, 9]. The surface-to-volume ratio is better, the stoichiometry is better, and the crystallinity is greater. In the filaments of lighting bulbs, tungsten was employed primarily because it is less efficient than other metals at converting energy into light. Because of this, it can swiftly harvest the visible light spectrum (450 nm) with a bandgap value of roughly 2.5 to 2.8 eV [10, 11]. In addition to having an excessive amount of oxidizing power in the form of valence band holes [12], it is one of the most prominent photocatalysts because it has no photo-attrition, fine electron transmission effects, excellent stability, and excessive photoactivity [13]. It is also chemically inert, thermally stable, and completely safe to use in any manner. It can store more photogenerated electrons and photogenerated holes with a high oxidation power thanks to its varied oxidation states [14, 15].

Although the monoclinic phase of tungsten trioxide is the most stable, temperature has an impact on the crystal structure. Mineralization into simple and harmless species with the ability to reduce processing costs is the main benefits of MB dye. Textile wastewaters are frequently highly coloured as a result of dyes that have been left behind. Methylene blue, which is used in businesses to colour paper, textiles, and hair, is also dangerous to human health. This is why repair and degradation are necessary to prevent MB's detrimental effects on our environment. Dye removal from liquid effluents can be achieved by photocatalytic degradation, which uses heterogeneous processes to break down the dyes [16]. Wet chemical precipitation, precipitation technique, sol-precipitation, sol-gel, surfactant pyrolysis, and the ion-exchange method are some of the ways used to aggregate tungsten trioxide [17]. WO_3 nanoparticles are made hydrothermally in this study and used as catalysts in the removal of methylene blue from the solution. Tungsten trioxide (WO_3) structure and methylene blue degradation are used to identify the produced nanoparticles [18, 19].

2. Experimental Section

2.1. Materials. Sodium tungstate, hydrochloric acid (HCl), and ethanol are procured from Sigma Aldrich, and deionized water is used for the preparation of WO_3 nanoparticles.

2.2. Synthesis of WO_3 Nanoparticles

$$Na_2WO_4 + 2HCl \longrightarrow WO_3 + 2NaCl + H_2O. \quad (1)$$

Sodium tungstate when reacting with hydrochloric acid gives a tungsten trioxide, for this preparation, we used sodium tungstate with the moles of 0.1, 0.2, and 0.3 named as W1, W2, and W3, respectively, were taken and dissolved in 50 ml of deionized water, and the mixture is magnetically stirred continuously until all the sodium tungstate were diffused completely. Then, HCl was added with caution in the above concoct solution; by adding the HCl dropwise, the white solution gets to turn into yellow and become viscous then it is filtrate to eliminate the excess HCl, by filtering, it we get a yellowish precipitate that then turns into an oven at 60°C for 24 h for dry. The material is powdered by mortar, and finally, we get WO_3 nanoparticles. Figure 1 shows the schematic diagram of the WO_3 nanoparticles using sodium tungstate. The crystal phase structure of WO_3 nanoparticles is shown in Table 1. Figure 2 shows the WO_3 nanopowder.

2.3. Characterization

2.3.1. X-Ray Diffraction (XRD). X-ray diffractometer (X-Pert Pro) with CuK radiation (1.5405) and a 2 range of 20°-80° was used to examine the crystal structure of WO_3 nanoparticles. With Scherrer's equation, the sample's grain size was derived from the full width at half maximum (FWHM) XRD peak areas.

Debye-Scherrer's equation,

$$D = K\frac{\lambda}{\beta}\mathrm{Cos}\Theta\,; \quad (2)$$

where D is the average crystalline domain size; β is the full width at half maximum (FWHM), $K = 0.94$, λ is the wave length, and Θ is the diffracted angle.

2.3.2. Fourier Transform Infra-Red Spectroscopy (FT-IR). The functional group of the WO_3 nanoparticles was analyzed using FTIR spectroscopy. It offers perceptible and every partial investigation for organic and inorganic samples. These measurements were carried using a PerkinElmer spectrum RX I FTIR instrument with a wavenumber range of 4000 to 400 cm. The shift in the functional peaks was compared for the result.

2.3.3. UV Spectrophotometric Analysis (UV-DRS). The spectral study of nanoparticles necessitates a detailed investigation of the process of their formation. The UV spectra of the chemically generated WO3 nanoparticles were measured using a Shimadzu UV-1800 spectrophotometer, with the wavelength range being 200 nm to 900 nm and BaSO4 serving as the baseline correction.

2.3.4. Field Emission Scanning Electron Microscope with Energy-Dispersive X-Ray Analysis (FE-SEM with EDX). The surface morphology was recorded using the Carl Zeiss SIGMA instrument. The FE-SEM image shows the WO_3 nanoparticles. The energy-dissipation of X-ray spectra

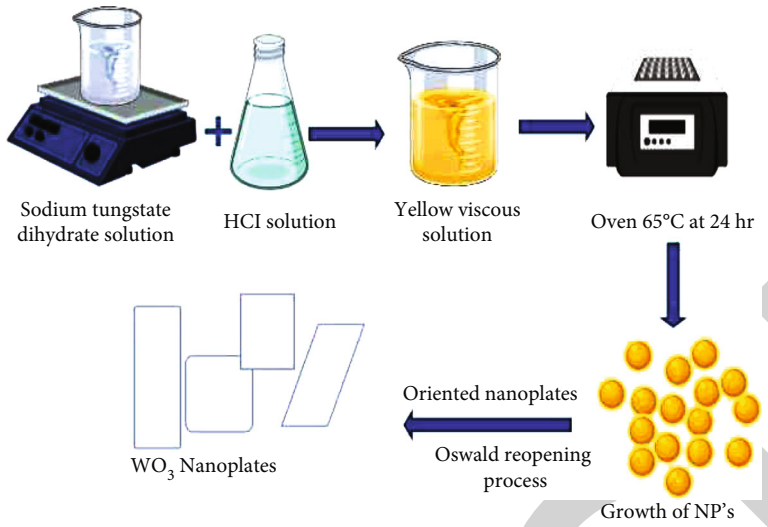

Figure 1: Schematic diagram of the WO_3 nanoparticles using sodium tungstate.

Table 1: Crystal phase structure of WO_3 nanoparticles.

nPos. [°2Th.]	Corresponding *h k l* planes			
	WO_3	W1	W2	W3
16.6°	0 1 1	0 1 1	0 1 1	0 1 1
25.8°	0 1 2	0 1 2	0 1 2	0 1 2
34.2°	2 0 2	2 0 2	2 0 2	2 0 2
35.1°	1 2 2	1 2 2	1 2 2	1 2 2
49.8°	1 4 0	1 4 0	1 4 0	1 4 0
52.8°	1 3 3	1 3 3	1 3 3	1 3 3
56.3°	2 4 1	2 4 1	2 4 1	2 4 1

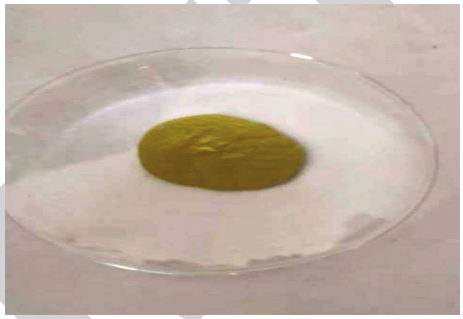

Figure 2: WO_3 nanopowder.

(EDX) was recorded using the INCAx-act Oxford device fit out with SEM.

2.3.5. Photocatalytic Activity. Methylene blue mixtures were used in our current study as a model dye outflow solution for degradation of the synthesized WO_3nanoparticles. MB is one of the well-known dyes used in the textile industry. Cationic methylene blue 3, 7-bis (dimethylamino)-phenothiazine-5-in chloride as well as tetramethyl thionine is an important synthetic dye with an average molecular weight of 319.85 grammes per mole 1. To further understand the relationship between catalytic activity and concentration, we investigated MB dye at three different NP concentrations. The activities were exposed under visible light (<400 nm) using xenon lamb. For that, 10 mg of the photocatalyst was mixed with methylene blue dye of 100 ml. For the adsorption/desorption equilibrium to be achieved, the mixture was agitated magnetically for one hour in the dark. By exposing the suspension to xenon light, the degradation was started, 3 ml of suspended solution was taken out at regular time intervals of every 30 mins; then, it is centrifuged and analyzed using UV-Vis spectroscopy. The degradation absorption peaks at 666 nm. The following equation was used to estimate dye degradation.

$$\text{Degradation}(\%) = \left(C_0 - \frac{C_t}{C_0}\right) \times 100 \quad (3)$$

where C_0 is the initial absorption of the methylene blue dye solution, and C_t is the absorption of the dye solution after Xenon light exposure.

3. Results and Discussion

3.1. X-Ray Diffraction. XRD is a method that analyses the structure of the sample and its assemblage such as

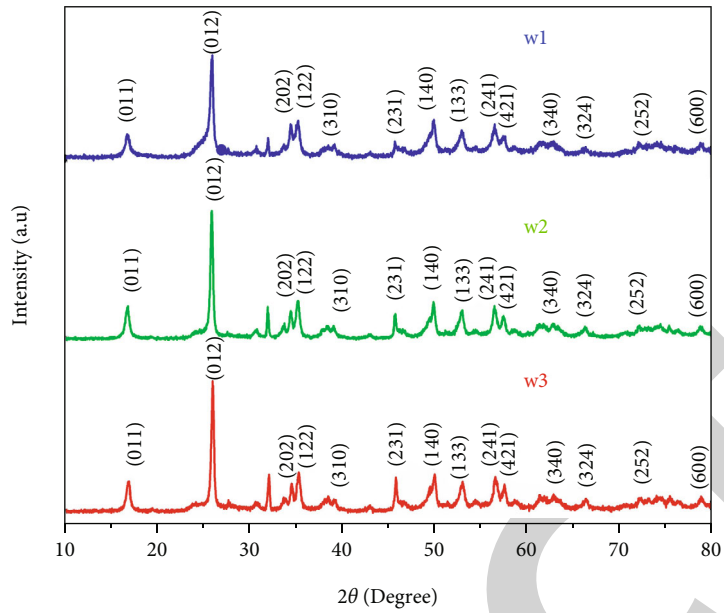

Figure 3: Crystal phase structure of WO_3 nanoparticles.Table 1 explains about crystal phase structure of WO_3 nanoparticles.

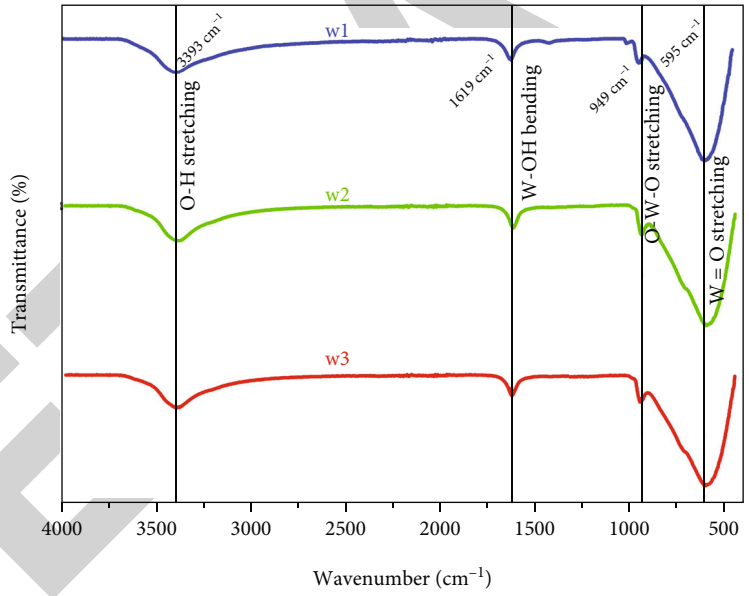

Figure 4: FT-IR spectrum of WO_3 nanoparticles.

microstrain, crystalline size, and dislocation density, and it is making use of point out the attribute about appearance compositions crystal favoured direction and crystal defect concentrations [20]. Figure 3 shows a crystal phase structure of WO_3 nanoparticles. The presence of intense peaks confirmed the highly crystalline structure of WO_3 nanoparticles observed at $2\theta = 16.6^\circ$, 25.8°, 34.2°, 35.1°, 49.8°, 52.8°, and 56.3°, these are the firm peaks which are associated with the (011), (012), (202), (122), (140), (133), and (241) crystalline planes of WO_3 with good crystallization, and they appear in good consensus with the monoclinic system in the JCPDF (83-0950) [21]. Some unwanted peaks are coming from the source material. For a better crystallinity, the strength of the peaks needs more extreme and sharper, and our sample has this condition. The grain size of high-intensity peaks was evaluated using Debye Scherrer formula. The average crystallite size is around 34 nm for all samples.

3.2. Fourier Transform Infra-Red Spectroscopy. The Fourier transform infrared spectroscopy (FT-IR) gives the information of chemical bonds of the compound. It is demonstrated in Figure 4 that 4000–500 cm-1 WO_3 nanoparticles have an FTIR spectrum. Broadband 3400-3200 cm-1 that can be ascribed to O–H stretching vibrations from the absorbed water may be identified [22]. The weak peaks located at 1618 cm^{-1} indexed to O–H bending modes of absorbed

water [23, 24]. A small and sharp peak at 940 cm^{-1} is indexed to W=O stretching mode [25]. The broadband at 595 to 610 cm^{-1} indicates the O-W stretching modes indicate the formation of tungsten [26]. These indicate the metal oxide stretching, vibration (M-O_6). The vital absorption region of 600–1000 cm^{-1} shows nonidentical morphologies existing various sidebars of the infrared spectrum, and also, it is the features of O-W-O stretching vibrations in the WO_3 crystal lattice. From the FT-IR, we conclude that WO_3 nanoparticles are well immersed with our samples, and it is well evidenced with the XRD spectrum.

Table 2 shows the FTIR spectra.

3.3. UV-Visible Spectroscopy. The optical measurements were carried by UV-DRS spectrometer. Figure 5(a) shows the reflectance spectrum of WO_3 nanoparticles. All our samples exhibit clear peaks and absorption boundary within the visible range of 400 to 500 nm, which was prompt by the transmission of an electron from the VB to the CB and also accepted that the samples could absorb visible light in the UV-region [27] that corresponds to the rudiment absorption of WO_3 semiconductor. Tauc's equation calculates the bandgap energies of the sample.

$$\alpha h\upsilon = ((h\upsilon - E))^n. \quad (4)$$

α is the absorption coefficient. υ is the frequency. E_g is the bandgap. $n - 0.5$ is the direct bandgap semiconductor.

Generally, the absorbance depends on optical bandgap and impurity centers. For indirect transition by plotting $(\alpha h\upsilon)^2$ versus $(h\upsilon)$, we can find the energy of the sample (Figure 5(b)). The straight-line intercept of the x-axis gives the bandgap value of the WO_3 nanoparticles, 2.52 eV, 2.36 eV, and 2.51 eV for W1, W2, and W3 nanoparticles, respectively. The WO_3 bandgap energy is calculated to be around 2.4 eV utilizes the formula $E_g = 1240/\lambda$, where λ is absorption wavelength of 514 nm; from this, we confirmed that indirect transition gives the perfect bandgap values of the WO_3 nanoparticles. As we know, the base bandgap of photocatalysts must be 1.23 eV, and also a successful photocatalyst has been evincing bandgaps larger than 2 eV, lower the bandgap greater the efficiency. Therefore, our samples have a lower bandgap which satisfies the catalytic activity, compared to other two samples, W2 has small bandgap and so it is taken for the different characteristics to get a better morphology, binding energy and degradations.

3.4. Field Emission Scanning Electron Microscopy (FE-SEM). FE-SEM is to acquire information about the texture, shape, and size of WO_3 nanoparticles. Figure 6 shows the different magnified images of the WO_3 nanoparticles (W2) prepared by hydrothermal process and calcination with a 60°C for 24 hours. WO_3 powder is composed of a significant number of square nanoplates [28] with a length of 232.6 nm, in addition to the fact that there are many variances in the form and length of the nanoplates produced in our sample. It is a monodispersive much nanoplate with the primary distribution of tungsten. It consists of oxygen, so we have sharp edges in every nanoplate. It is confirmed by elemental mapping. The mapping images reassure the oxygen distribution with the tungsten surface.

Table 2: FTIR spectra.

Bond	Wave number
O-H	3393 cm^{-1}
W-OH	1619 cm^{-1}
O-W-O	949 cm^{-1}
W=O	595 cm^{-1}

The configuration and elemental scanning of the calcined WO_3 (W2) powder was analyzed by EDX spectra in the energy range between 0 and 10 KeV. Figure 7 shows the EDX spectrum of the sample. Our sample's spectrum clearly shows facet peaks of tungsten (W M) as well as oxygen (O K) atoms, and nonappearance of any other peaks shows the exclusive tungsten oxide phase which is a sign of high purity WO_3 without any elemental impurities in the preparation and calcining process.

3.5. X-Ray Photoelectron Spectroscopy. X-ray photoelectron spectroscopy (XPS) is examined to find out the surface composite and elemental valence of the WO_3 samples (W2) in Figure 8.

The broad scan spectra (Figure 8(a)) show the apparent signals of W4f, W4$d_{5/2}$, W4$d_{3/2}$, W4$p_{3/2}$, C1s, and O1s at 37.2, 247.37, 259.34, 425.96, 284.4, and 531.1 eV, respectively. In the O1s spectra (Figure 8(b)), the peak at 531.6 eV can be associated with oxygen bonded to metal species and is the signal from O-1 state, whereas the other peak at 532.91 eV is referred as O in H_2O and W-O-H [29, 30]. The unpremeditated carbon is present in every XPS instrument the peak at 284.5 eV shows the C1s (Figure 8(c)) [31]. The W4f spectrum is split into states each state has a couple of doublets after succeeding thresholding of the high-resolution spectrum. The pinnacle in W4f spectra (Figure 7(d)) centering at 36.01 eV and 38.1 eV is the features of W4$f_{7/2}$, W4$f_{5/2}$, respectively. The spin-orbital separation of the two peaks is 2.1 eV, which accede the conceptual value for WO_3 [32]. From the above results, the obtained binding energy confirms the presents of WO_3 nanoparticles, and it shows the various oxidation states.

3.6. Photocatalytic Activity. An equal or higher amount of photon energy than the bandgap of the photocatalyst is required for photocatalytic degradation. For that propound mechanism for WO_3 accommodates decay of MB replicated in visible light, the bandgap stimulation with the involvement of photons foremost to larger oxidant group in the aqueous media they show the photocatalytic decay of biological contaminant. The oxidation of H2O molecules by VB holes (h+) and reduction of dissolved oxygen by the conduction band electrons (e−) aggregate in the formation of hydroxyl (HO•) and superoxide anion radicals (O2•−). These hydroxyl radicals have well-built oxidizing power that is in charge of the degradation of pollutants and the electrons in the CB that react with dissolved oxygen groups

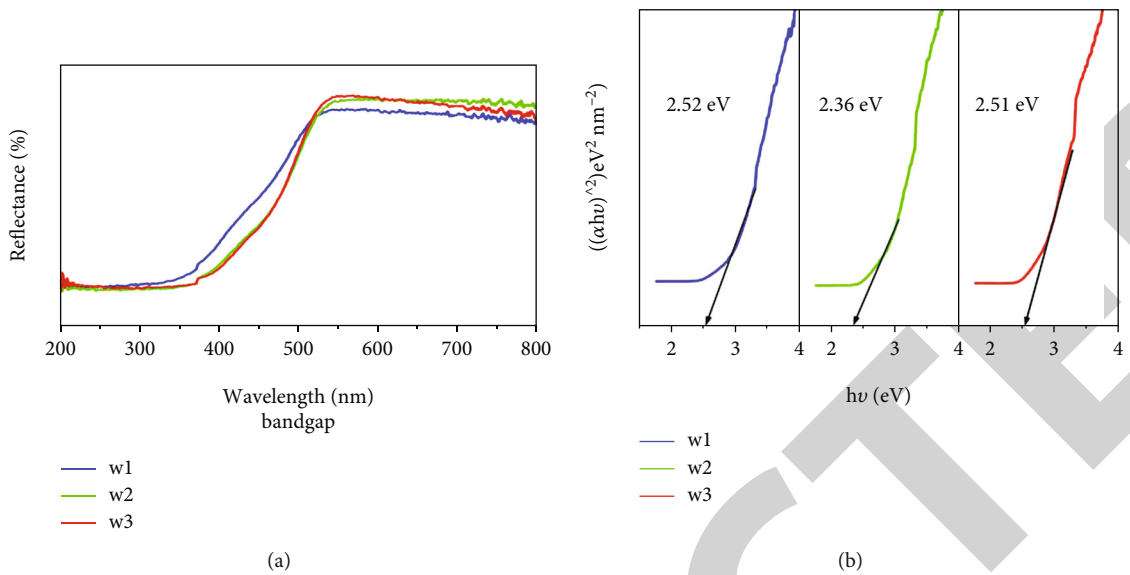

Figure 5: (a) Reflectance spectrum. (b) Tauc plot of WO_3 nanoparticles.

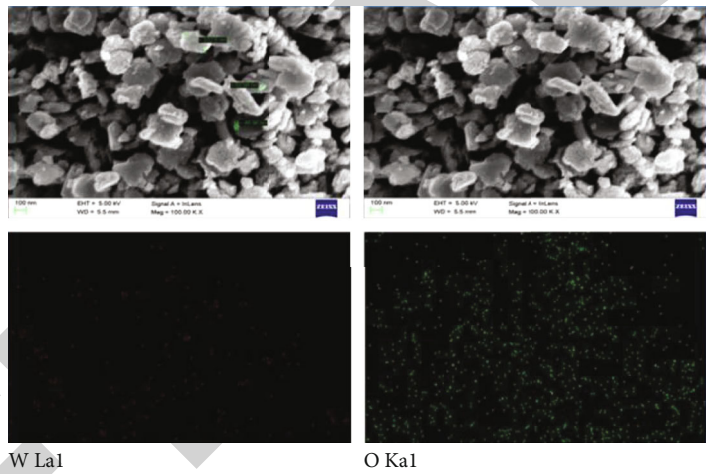

Figure 6: FE-SEM and mapping image of WO_3 nanoparticles.

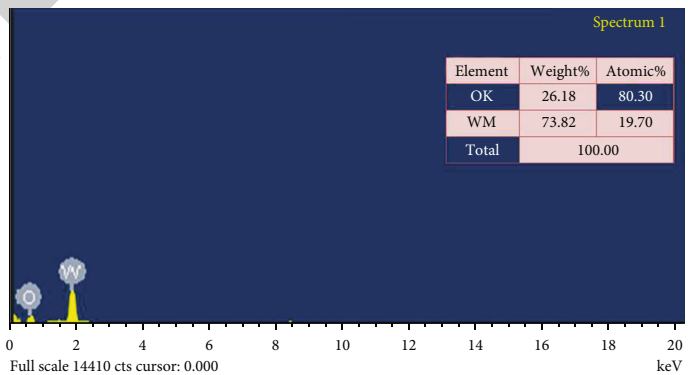

Figure 7: EDX image of prepared WO_3 nanoparticles.

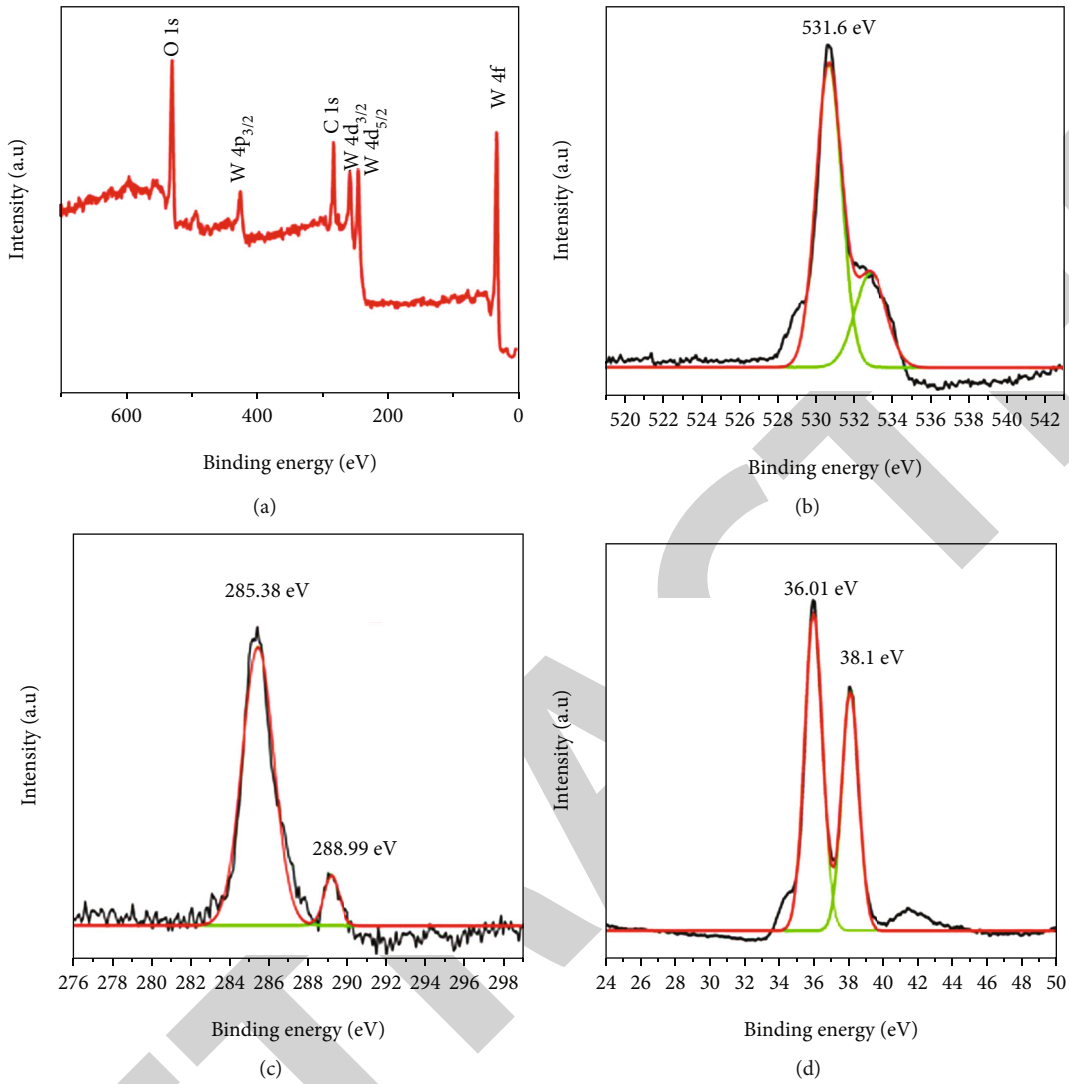

Figure 8: XPS image of prepared WO_3 nanoparticles (a) wide, (b) O1s, (c) C1s, and (d) W4f.

to form superoxide ions. These electrons persuade redox reactions, as presented in the set of equations below.

$$\begin{aligned} WO_3 + h\nu(E \geq Eg) &\longrightarrow e^- + h^+. \\ H_2O+ &\longrightarrow HO^\bullet + H^+, \\ O_2 + e^- &\longrightarrow O_2\bullet^-, \\ O_2\bullet-/OH + MB &\longrightarrow \text{Degraded molecules}. \end{aligned} \tag{5}$$

The improved mechanism for catalytic pursuit of WO_3 depends on severance and transmission of photogenerated charged carriers. The photocatalytic degradation process is carried out for WO_3 nanoparticles of various concentration. In order to determine the UV-spectroscopic absorbance for MB, measurements were taken over the photocatalysts that had been fabricated, as shown in Figure 9(a).

Methylene blue has strong absorption bands at 291 nm and 664 nm, which progressively decrease as the irradiation period is prolonged. Methylene blue is a colourless liquid. A photocatalyst (for example, methylene blue) may be employed to start the degradation or disappearance of MB when exposed to visible light. Decolorization of MB may be accomplished by either oxidative degradation or two-electron reduction [33]. We were able to find the leuco-MB absorption band at 291 nm, which was previously unknown. This suggests that colour fluctuations in MB are the result of the dye being degraded by oxygen in the air [34]. After 150 minutes, the amount of MB was utterly degraded (Figure 9(b)). From the degradation vs. time curve showing that W2 has high degradation efficiency compared to W1 and W3. The methylene blue catalytic degradation is evaluated by pseudofirst-order kinetics, from that the adsorption kinetics results W2 have higher kinetics (Figure 9(c)) as compared to the other two samples W1 and W3, and the calculated values are $0.0129 < 0.0141 > 0.0133$, respectively.

The schematic representation of WO_3 nanoparticle photocatalyst MB degradation is as shown in Figure 10.

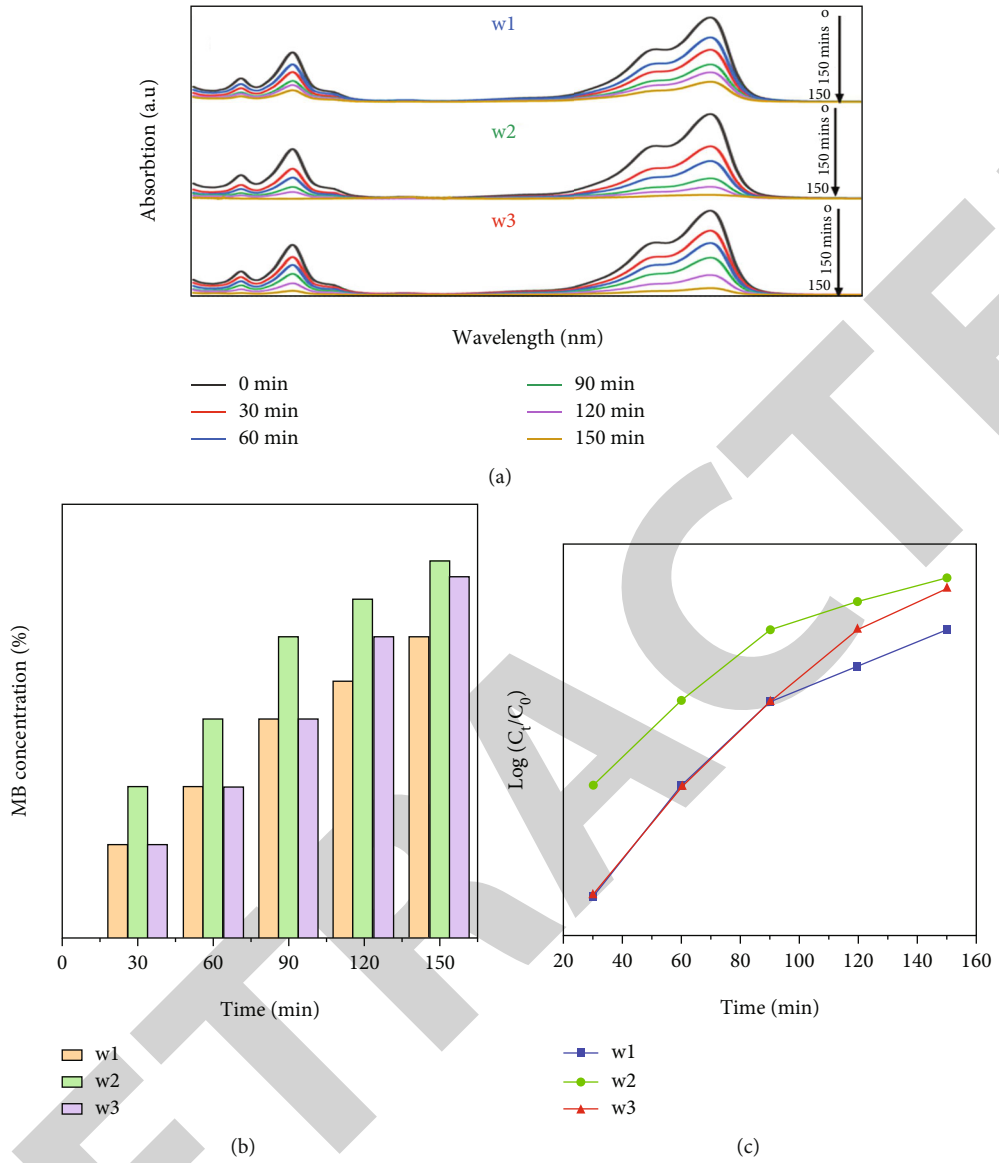

Figure 9: (a) UV-Vis spectra of methylene blue, (b) degradation concentration, and (c) kinetics study of WO_3 nanoparticles.

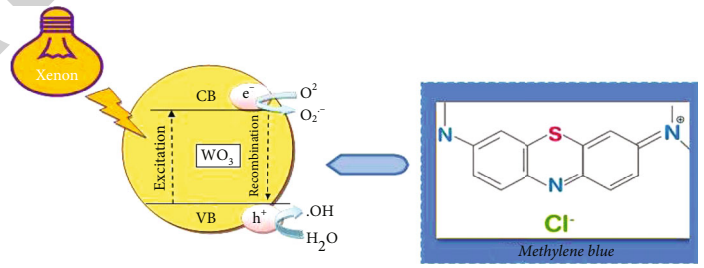

Figure 10: Photocatalyst dye degradation of WO_3 nanoparticles.

4. Conclusion

(1) The hydrothermal approach was used to create WO_3 nanoparticles, as was stated in this research paper

(2) The findings of the XRD experiment point to the development of WO_3 crystals that have a monoclinic structure

(3) In addition, the bandgap energy may be determined from the UV-Vis DRS spectra of the WO_3 nanoparticles

(4) Studies using a scanning electron microscope showed nanoplates that were the same length as the WO_3 nanoparticles

(5) The EDX analysis verifies that the sample contains sodium and oxide in the appropriate amounts

(6) The XPS results that were obtained for the binding energy support the presence of WO_3 nanoparticles, and they also demonstrate the different stages of oxidation

(7) The photocatalytic activity of WO_3 nanoparticles has been shown to successfully destroy methylene blue when exposed to xenon light. It is validated by UV-DRS because the onset absorbance value offers a great bandgap value of the tungsten trioxide. Comparing sample w2 to sample w1 and sample w3 shows that sample w2 has a higher level of deposition. In light of these findings, it is clear that WO_3 nanoparticles play an important part in the degradation of methylene blue dye, and that the mechanism involved in doing so is convenient and economical for use in both medical and industrial settings

Data Availability

The data used to support the findings of this study are included in the article.

Conflicts of Interest

The authors declare that they have no conflicts of interest regarding the publication of this paper.

References

[1] C. S. C. Santos, B. Gabriel, M. Blanchy et al., "Industrial applications of nanoparticles - a prospective overview," *Materials Today*, vol. 2, no. 1, pp. 456–465, 2015.

[2] I. Khan, K. Saeed, and I. Khan, "Nanoparticles: properties, applications and toxicities," *Arabian Journal of Chemistry*, vol. 12, no. 7, pp. 908–931, 2019.

[3] J. Huang, J. Liu, and J. Wang, "Optical properties of biomass-derived nanomaterials for sensing, catalytic, biomedical and environmental applications," *TrAC Trends in Analytical Chemistry*, vol. 124, article 115800, 2020.

[4] S. M. Hassan, A. I. Ahmed, and M. A. Mannaa, "Preparation and characterization of SnO_2 doped TiO_2 nanoparticles: effect of phase changes on the photocatalytic and catalytic activity," *Journal of Science: Advanced Materials and Devices*, vol. 4, no. 3, pp. 400–412, 2019.

[5] A. M. Nasir, J. Jaafar, F. Aziz et al., "A review on floating nanocomposite photocatalyst: fabrication and applications for wastewater treatment," *Journal of Water Process Engineering*, vol. 36, article 101300, 2020.

[6] S. D. Marshal Dhayal, C. K. Sharma, K. K. Saini, and S. C. Jain, "Role of Ni doping in surface carbon removal and photo catalytic activity of nano-structured TiO_2 film," *Surface Science*, vol. 602, no. 6, pp. 1149–1154, 2008.

[7] D. Chatterjee and S. Dasgupta, "Visible light induced photocatalytic degradation of organic pollutants," *Journal of Photochemistry and Photobiology C: Photochemistry Reviews*, vol. 6, no. 2-3, pp. 186–305, 2005.

[8] T. G. G. Maffeis, D. Yung, L. Lepennec et al., "STM and XPS characterisation of vacuum annealed nanocrystalline WO_3 films," *Surface Science*, vol. 601, no. 21, pp. 4953–4957, 2007.

[9] O. Hurtado-Aular, A. B. Vidal, A. Sierraalta, and R. Añez, "Periodic DFT study of water adsorption on m-WO_3(001), m-WO_3(100), h-WO_3(001) and h-WO_3(100). Role of hydroxyl groups on the stability of polar hexagonal surfaces," *Surface Science*, vol. 694, article 121558, 2020.

[10] S. Supothina, P. Seeharaj, S. Yoriya, and M. Sriyudthsak, "Synthesis of tungsten oxide nanoparticles by acid precipitation method," *Ceramics International*, vol. 33, no. 6, pp. 931–936, 2007.

[11] J. Yu and L. Qi, "Template-free fabrication of hierarchically flower-like tungsten trioxide assemblies with enhanced visible-light-driven photocatalytic activity," *Journal of Hazardous Materials*, vol. 169, no. 1-3, pp. 221–227, 2009.

[12] N. Asim, M. F. Syuhami, M. Badiei, and M. A. Yarmo, "WO_3 modification by synthesis of nanocomposites," *APCBEE Procedia*, vol. 9, pp. 175–180, 2014.

[13] Muhammad Yousaf Khan, "Visible light active indigo dye/graphene/WO_3 nanocomposites with excellent photocatalytic activity," *Journal of Materials Research and Technology*, vol. 8, no. 3, pp. 3261–3269, 2019.

[14] J. Zhu, J. He, L. Hu, and L. Da, "All-solid-state Z-scheme WO_3/$HTiNbO_5$-NS heterojunctions with enhanced photocatalytic performance," *Journal of Solid State Chemistry*, vol. 276, pp. 104–113, 2019.

[15] R. Wang, G. Qiu, Y. Xiao, X. Tao, W. Peng, and B. Li, "Optimal construction of $WO_3 \cdot H_2O$/Pd/CdS ternary Z-scheme photocatalyst with remarkably enhanced performance for oxidative coupling of benzylamines," *Journal of Catalysis*, vol. 374, pp. 378–390, 2019.

[16] Y. Yang, H. Zhong, C. Tian, and Z. Jiang, "Single-step preparation, characterization and photocatalytic mechanism of mesoporous Fe-doped sulfated titania," *Surface Science*, vol. 605, no. 13-14, pp. 1281–1286, 2011.

[17] A. M.-d. la Cruz, D. S. Martínez, and E. L. Cuéllar, "Synthesis and characterization of WO3 nanoparticles prepared by the precipitation method: evaluation of photocatalytic activity under vis-irradiation," *Solid State Sciences*, vol. 12, no. 1, pp. 88–94, 2010.

[18] K. Z. Elwakeel, A. A. El-Bindary, and E. Y. Kouta, "Retention of copper, cadmium and lead from water by Na-Y-Zeolite confined in methyl methacrylate shell," *Journal of the Chinese Chemical Society*, vol. 5, no. 4, pp. 3698–3710, 2017.

[19] P. Bijesh, V. Selvaraj, and V. Andal, "A review on synthesis and applications of nano metal oxide/porous carbon composite," *Materials Today: Proceedings*, vol. 55, pp. 212–219, 2022.

[20] K. Buvaneswari, G. Vetha, and V. Andal, "Green synthesis of ZnAl2O4 nanoparticles for the degradation of methyl orange dye under visible light," *International Journal of ChemTech Research*, vol. 8, pp. 06–09, 2015.

[21] S. R. Bathe and P. S. Patil, "WO_3 thin films doped with Ru by facile chemical method with enhanced electrochromic

properties for electrochromic window application," *Materials Science and Engineering: B*, vol. 257, article 114542, 2020.

[22] W. S. A. El-Yazeed and A. I. Ahmed, "Photocatalytic activity of mesporous WO_3/TIO_2 nanocomposites for the photodegradation of methylene blue," *Inorganic Chemistry Communications*, vol. 105, pp. 102–111, 2019.

[23] J. Yao, M. Zhang, H. Yin, Y. Luo, and X. Liu, "Improved photocatalytic activity of WO_3/C_3N_4: by constructing an anchoring morphology with a Z-scheme band structure," *Solid State Sciences*, vol. 95, article 105926, 2019.

[24] X. Zhang, R. Zhang, S. Niu, J. Zheng, and C. Guo, "Construction of core-shell structured $WO_3@SnS_2$ hetero-junction as a direct Z-scheme photo-catalyst," *Journal of Colloid and Interface Science*, vol. 554, pp. 229–238, 2019.

[25] N. Omrani and A. Nezamzadeh-Ejhieh, "Photodegradation of sulfasalazine over Cu_2O-$BiVO_4$-WO_3 nano-composite: characterization and experimental design," *International Journal of Hydrogen Energy*, vol. 45, no. 38, pp. 19144–19162, 2020.

[26] S. Salmaoui, F. Sediri, N. Gharbi, C. Perruchot, and M. Jouini, "Hexagonal hydrated tungsten oxide nanomaterials: hydrothermal synthesis and electrochemical properties," *Electrochimica Acta*, vol. 108, pp. 634–643, 2013.

[27] L. Song, D. liu, S. Zhang, and J. Wei, "WO_3 cocatalyst improves hydrogen evolution capacity of ZnCdS under visible light irradiation," *International Journal of Hydrogen Energy*, vol. 44, no. 31, pp. 16327–16335, 2019.

[28] B. Miao, W. Zeng, Y. Mu et al., "Controlled synthesis of monodisperse $WO_3 \bullet H_2O$ square nanoplates and their gas sensing properties," *Applied Surface Science*, vol. 349, pp. 380–386, 2015.

[29] S. Q. Yu, Y. H. Ling, J. Zhang, F. Qin, and Z. J. Zhang, "Efficient photoelectrochemical water splitting and impedance analysis of WO_{3-x} nanoflake electrodes," *International Journal of Hydrogen Energy*, vol. 42, no. 32, pp. 20879–20887, 2017.

[30] J. Jia, C. Jiang, X. Zhang et al., "Urea –modified carbo quantum dots as electron mediator decorated $g\text{-}c_3n_4/WO_3$ with enhanced visible-light photocatalytic activity and mechanism insight," *Applied Surface Science*, vol. 495, article 143524, 2019.

[31] S. Sharma and S. Basu, "Highly reusable visible light active hierarchical porous WO_3/SiO_2 monolith in centimeter length scale for enhanced photocatalytic degradation of toxic pollutants," *Separation and Purification Technology*, vol. 231, article 115916, 2020.

[32] M. Dhanalakshmi, S. Lakshmi Prabavathi, K. Saravanakumar, B. Filip Jones, and V. Muthuraj, "Iridium nanoparticles anchored WO_3 nanocubes as an efficient photocatalyst for removal of refractory contaminants (crystal violet and methylene blue)," *Chemical Physics Letters*, vol. 745, article 137285, 2020.

[33] M. H. H. Mahmoud, A. A. Ismail, and M. M. S. Sanad, "Developing a cost-effective synthesis of active iron oxide doped titania photocatalysts loaded with palladium, platinum or silver nanoparticles," *Chemical Engineer*, vol. 187, pp. 96–103, 2012.

[34] A. A. Ismail, M. Faisal, and A. Al-Haddad, "Mesoporous WO_3-graphene photocatalyst for photocatalytic degradation of methylene blue dye under visible light illumination," *Journal of Environmental Sciences*, vol. 66, pp. 328–337, 2018.